Fatigue & Fracture of Engineering Materials & Structures

doi: 10.1111/ffe.12157

A single parameter to evaluate stress state in rail head for rolling contact fatigue analysis

C. L. PUN[1], Q. KAN[2], P. J. MUTTON[3], G. KANG[2] and W. YAN[1]

[1]*Department of Mechanical and Aerospace Engineering, Monash University, Clayton, VIC 3800, Australia,* [2]*Department of Applied Mechanics and Engineering, Southwest Jiaotong University, Chengdu, 610031, China,* [3]*Institute of Railway Technology, Monash University, Clayton, Vic 3800, Australia*

Received Date: 25 September 2013; Accepted Date: 27 December 2013; Published Online: 7 February 2014

ABSTRACT Based on the Smith-Watson-Topper (SWT) method, a phenomenological approach for multiaxial fatigue analysis, the maximum SWT parameter is proposed as a single parameter to evaluate the stress state in the rail head for assessing the fatigue integrity of the structure. A numerical procedure to calculate the maximum SWT parameter from a finite element analysis is presented and applied in a case study, where the stress and strain fields due to wheel/rail rolling contact are obtained from a three-dimensional finite element simulation with the steady-state transport analysis technique. The capability of the SWT method to predict fatigue crack initiation in the rail head is confirmed in the case study. Analogous to von Mises stress for strength analysis, the maximum SWT parameter can be applied to evaluate the fatigue loading state not only in rail head due to rolling contact fatigue but also in a generic structure subjected to a cyclic loading.

Keywords stress state in rail head; rolling contact fatigue; SWT method; maximum SWT parameter; finite element modelling.

NOMENCLATURE

$\Delta\varepsilon_e =$ elastic strain range
$\Delta\varepsilon_p =$ plastic strain range
$\Delta\varepsilon =$ normal strain range
$N_f =$ fatigue life
$b =$ fatigue strength exponent
$c =$ fatigue ductility exponent
$\sigma_f^{'} =$ fatigue strength coefficient
$E =$ elastic modulus
$\varepsilon_f^{'} =$ fatigue ductility coefficient
$\sigma_{max} =$ maximum normal stress
$\sigma_{11}, \sigma_{22}, \sigma_{33} =$ normal stresses
$\tau_{xy}, \tau_{yz}, \tau_{xz} =$ shear stresses
$\varepsilon_{xx}, \varepsilon_{yy}, \varepsilon_{zz} =$ normal strains
$\gamma_{xy}, \gamma_{yz}, \gamma_{xz} =$ shear strains
$n =$ unit normal to the candidate critical plane
$n_x, n_y, n_z =$ direction cosines of unit normal n
$\sigma^{'} =$ critical plane normal stress
$\varepsilon^{'} =$ critical plane normal strain
$S^{WT} =$ Smith-Watson-Topper parameter
$S^{WT}_{max} =$ maximum Smith-Watson-Topper parameter
$\theta_i =$ candidate critical plane angles
$x =$ running direction along the rail head
$y =$ transverse direction across the rail head
$h =$ the depth of the rail head
C1, C2 $=$ the two crack surfaces

Correspondence: Wenyi Yan. E-mail: wenyi.yan@monash.edu

INTRODUCTION

The demanding conditions imposed by rail transport with higher axle loads and increasing annual haulage rates lead to increased rates of rail degradation, such as wear and rolling contact fatigue. Although these situations can be mitigated by the development and application of higher strength rail steels, rolling contact fatigue, for example, in the form of dense surface cracks as shown in Fig. 1, is commonly found on the rail, especially in heavy haul railways, because of the combination of high axle loads and frequent train operations.[1] Therefore, the study of the degradation behaviour of rail steel has become an attractive research field in recent years. Some experimental studies and field observations[2–6] reported that the rolling contact fatigue strength/behaviour is dependent on rail grades, microstructure, composition and hardness of the rail steels. For instance, the improvement of the wear resistance by increasing the carbon content of the rail steels can influence the relative rates at which wear and rolling contact fatigue damage occur in rail head, and in some cases alter the morphology of the rolling contact fatigue damage. Additionally, Cookson and Mutton[7] found that the environmental factors play an important role in rolling contact fatigue cracking processes.

Basically, development of rolling contact fatigue damage can be divided into three stages, (i) initiation of cracks; (ii) crack propagation; and (iii) final failure. Among these three stages, prediction of fatigue crack initiation due to wheel/rail rolling contact is of foremost interest in railway management. First of all, such a theoretical analysis is applicable to prolonging the life for fatigue crack initiation. Second, the results of the prediction incorporating the analysis of crack propagation can be applied to estimate the appropriate rail grinding interval, which relies on the quantitative information of wear and rolling contact fatigue development. As rolling contact fatigue is a stress-related damage phenomenon, it is essential to investigate and quantify the stress state in the rail head by conducting stress analysis. Additionally, the results of the stress analysis can be used to design experimental tests, such as cyclic bi-axial compression-torsion test, in order to obtain the material parameters for the study of the ratcheting behaviour of rail steels using a three-dimensional cyclic plastic model.

Fig. 1 Dense surface cracks on the surface of the rail head in a heavy haul rail.[1]

Tournay *et al.*[8] have identified controlling the stress state in the rail head as of importance. Appropriate control of stress state of the railway can not only prevent unexpected failure, such as rolling contact fatigue damage, but also improve the life of both wheel and rail and the service reliability.[9] Fröhling[10] also emphasises that the stress state at the wheel/rail interface must be controlled within an acceptable limit for safer and more cost effective railway operations. Some previous studies were carried out to analyse the contact stresses or the stress field in the rail head under different rolling contact conditions. Influence of the tangential surface traction on the contact stresses was investigated by Jiang *et al.*.[11] Xu and Jiang[12] and Wen *et al.*[13] studied the influence of partial slip conditions in the contact area on the stress field in the rail using two-dimensional and three-dimensional finite element model, respectively. Study of the stress distribution on the white etching layer on rail head was carried out using two-dimensional finite element model by Seo *et al.*.[14] The influence of non-steady rolling contact on the contact stresses was investigated by Wen *et al.*.[15] Mutton *et al.*[1] also investigated the influence of loading conditions and increased head loss on longitudinal stresses in the rail head and the tendency for rolling contact fatigue cracks to cause rail failure.

Although the importance of controlling the stress state of the railway has been highlighted, most of the stress analyses conducted so far aimed to study the influence on either the contact stresses or the stress field in the rail head, which could be extracted from the finite element simulation directly. The basic question of how to evaluate the stress state in the rail head due to cyclic rolling contact for the assessment of structural integrity of the rail has not been fully investigated yet. Clearly, von Mises stress, which is used to evaluate the stress state for strength analysis of a structure, is not suitable for purpose for fatigue analysis of a structure under cyclic loading. The objective of this research is to identify a single parameter to evaluate the stress state in the rail head during actual rolling contact situations without carrying out a complicated fatigue life analysis. Such a parameter should have the capacity to correctly characterise the possible rail degradation level, such as the initiation of rolling contact fatigue.

The Smith-Watson-Topper (SWT) method,[16] which considers stress, elastic strain and plastic strain components, has demonstrated the capacity to predict the location, the orientation of crack initiation and the fatigue life of a structure under multiaxial cyclic loading, for example,[17] and [18] Additionally, Klemenc *et al.*[19] combined the SWT method as an analytical model with a hybrid multi-layer perceptron to model the dependency of the SWT damage parameter on the number of cycles to fatigue failure. To improve the accuracy for the estimation of multiaxial fatigue life, two fatigue damage models, were successfully developed by modifying the SWT method.[20,21] Therefore, the maximum SWT parameter from the SWT method for fatigue analysis is proposed to effectively evaluate the stress state in the rail head in the paper. A case study indicates that this parameter and the SWT method have the capability to not only evaluate the stress state but also predict the initiation of fatigue crack in the rail head.

The structure of this paper is as follows. The SWT method for rolling contact fatigue analysis, which corresponds to the maximum SWT parameter, is briefly described in the section on SWT Method for Rolling Contact Fatigue Analysis and the Maximum SWT Parameter. The finite element model and the numerical results from the SWT method in a case study is presented and discussed in the section on Numerical Example. Conclusions are given in the last section.

SWT METHOD FOR ROLLING CONTACT FATIGUE ANALYSIS AND THE MAXIMUM SWT PARAMETER

SWT method

Rolling contact fatigue is one of the two typical rail degradation modes. The other degradation mode, wear, is also the result of ratcheting mechanisms,[22] with the overall degradation of the rail reflecting the relative rates at which these two processes occur. Research has been extensively carried out to address all the three stages of rolling contact fatigue. Generally, two approaches, a phenomenological approach and a fracture mechanics approach, can be applied to study fatigue.[23] The aim of current research is to evaluate the stress state in rail head for assessing and controlling the rail integrity without carrying out a complicated fatigue life analysis. For this purpose, the phenomenological approach for fatigue analysis is adopted.

Socie[24] has reported that the SWT method can give a good correlation with in-phase and out-of-phase fatigue lives under multiaxial cyclic loadings. Some previous studies have already shown the applicability of the critical plane approach in the prediction of both crack plane and the fatigue life.[25,26] Ringsberg[27] proposed a fatigue parameter from a combined energy-density based and critical plane models to predict the fatigue life of wheel/rail cyclic loading. The SWT method in conjunction with the critical plane approach has also been successfully applied in a number of studies to predict the crack initiation and crack location of fretting specimens.[17,28–31] The SWT method in conjunction with the critical plane approach is applied to predict the fatigue resistance of the rail steel due to rolling contact in the rail head in current study. This method is briefly presented in the succeeding text.

The SWT method belongs to the strain-life phenomenological approach, which includes both elastic strain range and plastic strain range.[17] The contribution of the elastic strain range, $\Delta\varepsilon_e$, on the fatigue life, N_f is originally described by the Basquin's equation for high cycle fatigue,

$$\left(\frac{\Delta\varepsilon_e}{2}\right) = \frac{\sigma_f'}{E}\left(2N_f\right)^b \tag{1}$$

where σ_f' is the fatigue strength coefficient and b is the fatigue strength exponent. Under uniaxial compression-tension cyclic loading with the loading ratio as -1, Eq. (1) can be converted into the stress formula,

$$\sigma_{max} = \left(\frac{\Delta\varepsilon_e}{2}\right)E = \sigma_f'\left(2N_f\right)^b \tag{2}$$

where σ_{max} is the stress amplitude under the uniaxial compression-tension test. The contribution of the plastic strain range, $\Delta\varepsilon_p$, is originally described by the Coffin-Manson equation for low cycle fatigue,[17,23]

$$\left(\frac{\Delta\varepsilon_p}{2}\right) = \varepsilon_f'\left(2N_f\right)^c \tag{3}$$

where ε_f' is the fatigue ductility coefficient and c is the fatigue ductility exponent. The summation of Eqs. (2) and (3) gives the strain-life equation as follows,[23]

$$\frac{\Delta\varepsilon}{2} = \frac{\sigma_f'}{E}\left(2N_f\right)^b + \varepsilon_f'\left(2N_f\right)^c \tag{4}$$

The philosophy of the SWT method is to multiply the Basquin's formulation for maximum normal stress, Eq. (2), by the strain-life equation, Eq. (3), which leads to,

$$\sigma_{max}\frac{\Delta\varepsilon}{2}=\frac{\left(\sigma_f^{'}\right)^2}{E}\left(2N_f\right)^{2b}+\sigma_f^{'}\varepsilon_f^{'}\left(2N_f\right)^{b+c} \quad (5)$$

For a given material, the material coefficients, b, c and Young's modulus, E in Eq. (5) can be obtained from experimental tests. To apply the SWT method Eq. (5) to predict the fatigue life of a structure under three-dimensional cyclic loading, the following SWT parameter, S^{WT}, is introduced.

$$S^{WT}=\sigma_{\max}\frac{\Delta\varepsilon}{2} \quad (6)$$

For a given material point, $\sigma_{\max}$ is the maximum normal stress component in a specified direction during a fatigue loading cycle and $\Delta\varepsilon$ is the difference of the maximum and minimum normal strain components in the same specified direction during the loading cycle. Therefore, the parameter, S^{WT} is a function of the space orientation at a given material point. Among all the orientations, a maximum S^{WT}, denoted as $S^{WT}_{\max}$, can be found for this material point. Calculation should be carried out for the whole structure to search for the highest $S^{WT}_{\max}$ during the loading cycle. It is the highest $S^{WT}_{\max}$ that is then applied in Eq. (5) to predict the fatigue life to crack initiation in the structure, N_f. The location of the highest $S^{WT}_{\max}$ corresponds to the site of the fatigue crack initiation. The orientation corresponding to the highest $S^{WT}_{\max}$ at the critical site represents the normal direction of the predicted crack surface because the crack is normally perpendicular to the maximum normal stress component. The predicted crack surface was designated as the critical plane in the literature.[17]

Numerical procedure to determine the maximum SWT parameter

The parameter, S^{WT} can be calculated on the basis of stress and strain fields from a three-dimensional finite element analysis. The determination of the maximum SWT parameter $S^{WT}_{\max}$ in the SWT method from a finite element simulation for fatigue analysis requires some basic material parameters, such as elastic modulus E, yield strength Y, elastic Poisson's ratio v, which can be obtained from a relatively simple testing method, that is, the monotonic tensile test. The procedure to numerically determine the highest $S^{WT}_{\max}$ for wheel/rail rolling contact is shown in Fig. 2. The calculation starts from the identification of a critical zone, which is large enough to cover both large von Mises stress values and large principal strain values, for example, the top 30% to 40% of the von Mises stress values and of the maximum principal strain values. This is because the highest $S^{WT}_{\max}$ should be within a zone with large von Mises stress and large principal strain. After that, the values of the stress and strain components at the integrations points of the elements within the selected critical zone are collected. Three-dimensional critical plane implementation is then applied to define the direction cosines of a unit normal, n, to the candidate critical plane as described by Eqs. (7–9).[17]

$$n_x=-\sin\theta_v\sin\theta_h \quad (7)$$

$$n_y=\cos\theta_h \quad (8)$$

$$n_z=-\sin\theta_h\cos\theta_v \quad (9)$$

where θ_v and θ_h are the two angles to define the orientation of a specific candidate plane as shown in Fig. 3. Different candidate critical planes are considered by varying the angles of the plane from 0° to 360° with the increment of 5°. Three-dimensional stress and strain transformation as described by Eqs. (10) and (11) are then applied to determine the normal stress $\sigma^{'}$ and normal strain $\varepsilon^{'}$ to different candidate critical plane.

$$\sigma^{'}=\sigma_{xx}n_x^2+\sigma_{yy}n_y^2+\sigma_{zz}n_z^2+2\tau_{xy}n_xn_y+2\tau_{yz}n_yn_z+2\tau_{xz}n_xn_z \quad (10)$$

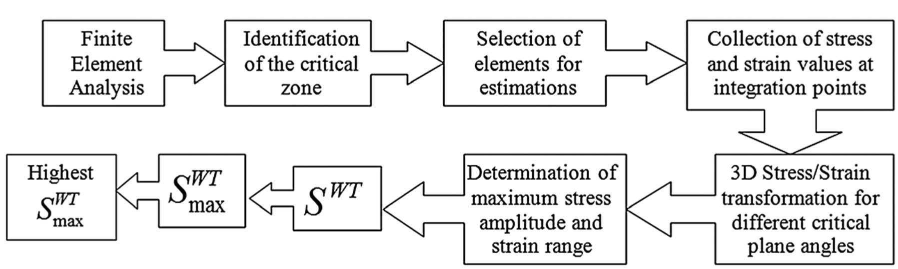

Fig. 2 Procedure to calculate the highest value of the maximum Smith-Watson-Topper parameter, $S^{WT}_{\max}$.

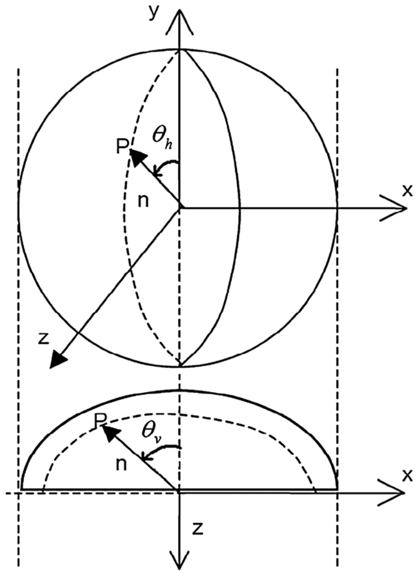

Fig. 3 Definition of angles θv and θb for calculating S^{WT}_{max}.[17]

$$\varepsilon' = \varepsilon_{xx}n_x^2 + \varepsilon_{yy}n_y^2 + \varepsilon_{zz}n_z^2 + 2\gamma_{xy}n_xn_y + 2\gamma_{yz}n_yn_z + 2\gamma_{xz}n_xn_z \qquad (11)$$

After that, the maximum normal stress component, σ_{max}, along the specified normal direction n, and the strain range, $\Delta\varepsilon$, which is the difference between the maximum and minimum values of the normal strain along the specified normal direction n, that is, the direction normal to the candidate critical plane of an integration point can be determined. Finally, multiplying the maximum stress amplitude by the strain range gives the S^{WT} value for each candidate critical plane. The plane which gives the maximum S^{WT} value, S^{WT}_{max} is the critical plane of that integration point. The same calculation should be repeated for all the integration points within the identified critical zone. The integration point that gives the highest S^{WT}_{max} value is the predicted location where the first fatigue crack will initiate in the structure. The critical plane at the critical integration point for the highest S^{WT}_{max} is the crack initiating surface of the predicted fatigue crack. A case study to determine the highest S^{WT}_{max} is presented in the next section.

NUMERICAL EXAMPLE

Finite element model

In this numerical example, the commercial finite element package Abaqus with the capability of steady-state transport analysis is used to simulate the wheel/rail contact under free rolling situation. The steady-state transport analysis technique applies the arbitrary Lagrangian Eulerian (ALE) formulation, which was developed by Nackenhorst,[32] to model rolling and sliding contact problems. As the ALE formulation is applied, this technique is a time-independent method. A steady moving contact is converted into a pure spatial problem by decomposing the total deformation of the rolling wheel into a rigid body motion and material deformation.[33,34] The rigid body motion is described by the Eulerian method while the material deformation is described by the Lagrangian method. Therefore, the dynamics of the wheel during rolling contact can be captured, although the rotating body does not undergo the large rigid body spinning motion. This method has been practically validated and some recent numerical studies of wheel/rail contact problems based on ALE formulation can be found in.[33,35]

A geometrically nonlinear three-dimensional finite element model is generated as shown in Fig. 4. The geometrical parameters of the wheel include the flange radius of 16 mm, the width of 145 mm, and the diameter of 965 mm; see Fig. 5. The technical parameters of the rail include the profile of a flat bottom rail, which has the mass of 68 kg/m with crown radius of 254 mm, gauge radius of 31.75 mm, and rail cant of 1/40; see Fig. 6.

The three-dimensional wheel model was generated by revolving an axisymmetric model of the wheel profile about its axis of revolution. The inner radius of the wheel is clamped to a reference point, which is located at the centre of the wheel. The normal load L, which is the axle load, is applied on that reference point; see Fig. 4. The

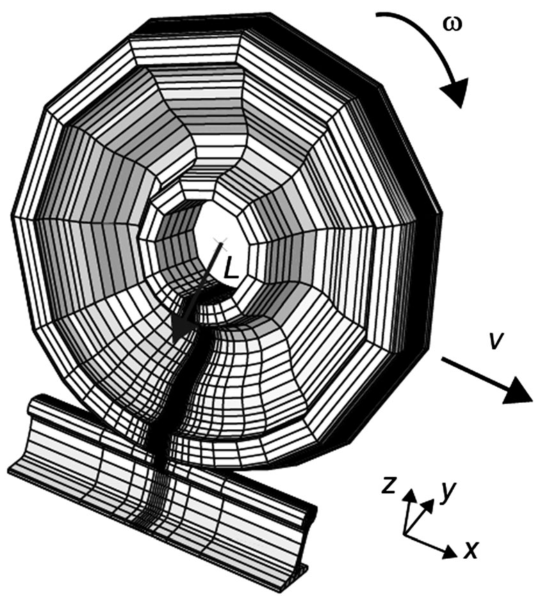

Fig. 4 Finite element model for simulating the steady-state wheel/rail rolling contact.

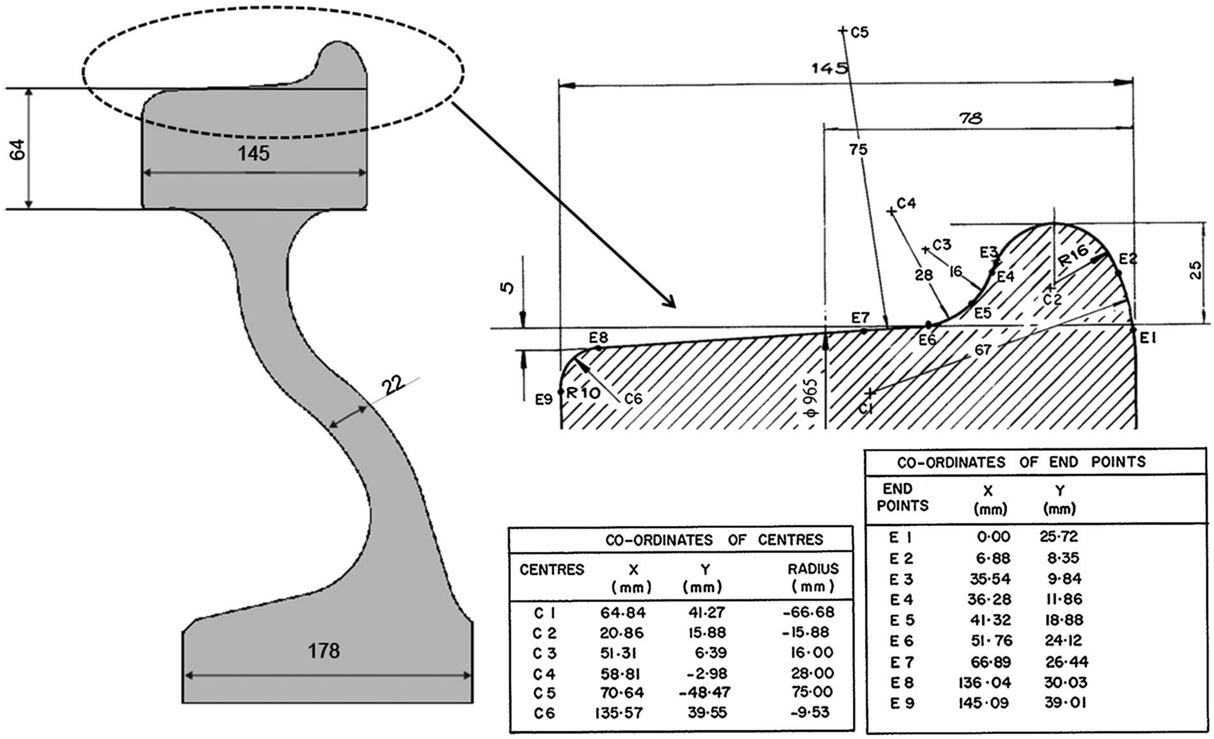

CO-ORDINATES OF CENTRES			
CENTRES	X (mm)	Y (mm)	RADIUS (mm)
C 1	64·84	41·27	-66·68
C 2	20·86	15·88	-15·88
C 3	51·31	6·39	16·00
C 4	58·81	-2·98	28·00
C 5	70·64	-48·47	75·00
C 6	135·57	39·55	-9·53

CO-ORDINATES OF END POINTS		
END POINTS	X (mm)	Y (mm)
E 1	0·00	25·72
E 2	6·88	8·35
E 3	35·54	9·84
E 4	36·28	11·86
E 5	41·32	18·88
E 6	51·76	24·12
E 7	66·89	26·44
E 8	136·04	30·03
E 9	145·09	39·01

Fig. 5 Cross-section of the wheel profile.

spinning motion of the wheel about its axis and the translational motion of the wheel with respect to the rail are denoted as ω and v, respectively, as illustrated in Fig. 4. The initial contact position between the wheel and the rail, which is the origin of the global coordinate system of the model, is calibrated by using a commercial mathematical software package MATLAB. The origin point (0,0,0) is used as the reference for presenting the results in following sections. The three-dimensional rail model was generated by extruding a two-dimensional rail profile. The mesh at the contact zone is refined in order to obtain accurate stress and strain results while coarse mesh is applied to the other part of the rail model in order to reduce the computational time. The surface-based mesh tie constraint, which makes the active degrees of freedom equal for a pair of surfaces with uneven mesh densities,[34] was applied to connect low and high density mesh regions. The wheel-rail finite element model consists of 88 631 C3D8 elements and it has 290 643 degrees of freedom in total.

Both wheel and rail are treated as deformable body, and they are described by the classical von Mises elastic-plastic constitutive material model with the consideration of isotropic hardening throughout the analysis. The Young's modulus and yield strength for the rail are 207 GPa and 751 MPa while those for the wheel are 210 GPa and 910 MPa. The Poisson's ratio and the work hardening exponent for both wheel and rail are 0.3 and 0.05, respectively. Coulomb friction law, which relates the frictional stresses to the slip velocity, is used as the friction model.[34]

Numerical results and discussion

The SWT method, which considers the effect of elastic strain, plastic strain and stress, incorporating critical plane approach is proposed to fully evaluate the stress state in the rail head. Following Fig. 2, the results and the details to determine the highest maximum SWT parameter, $S_{\max}^{WT}$ in the rail head of this wheel/rail rolling contact example under heavy haul loading situation are presented in the succeeding text.

Based on the finite element analysis, the von Mises stress and the maximum principal strain fields in the rail head for a free rolling case of friction coefficient of 0.3, and axle load of 30 t are shown in Figs. 7 and 8, respectively. The maximum von Mises stress zone is consistent with the maximum principal strain zone. Importantly, the critical zone for the SWT calculation can be determined as the zone with the top 35% of the von Mises stress values, which is outlined in Fig. 9. It is worth mentioning that the critical zone must be reasonably large to cover both large von Mises stress values and the large principal strain values if the large von Mises stress zone is not consistent with the large principal strain zone. After that, all

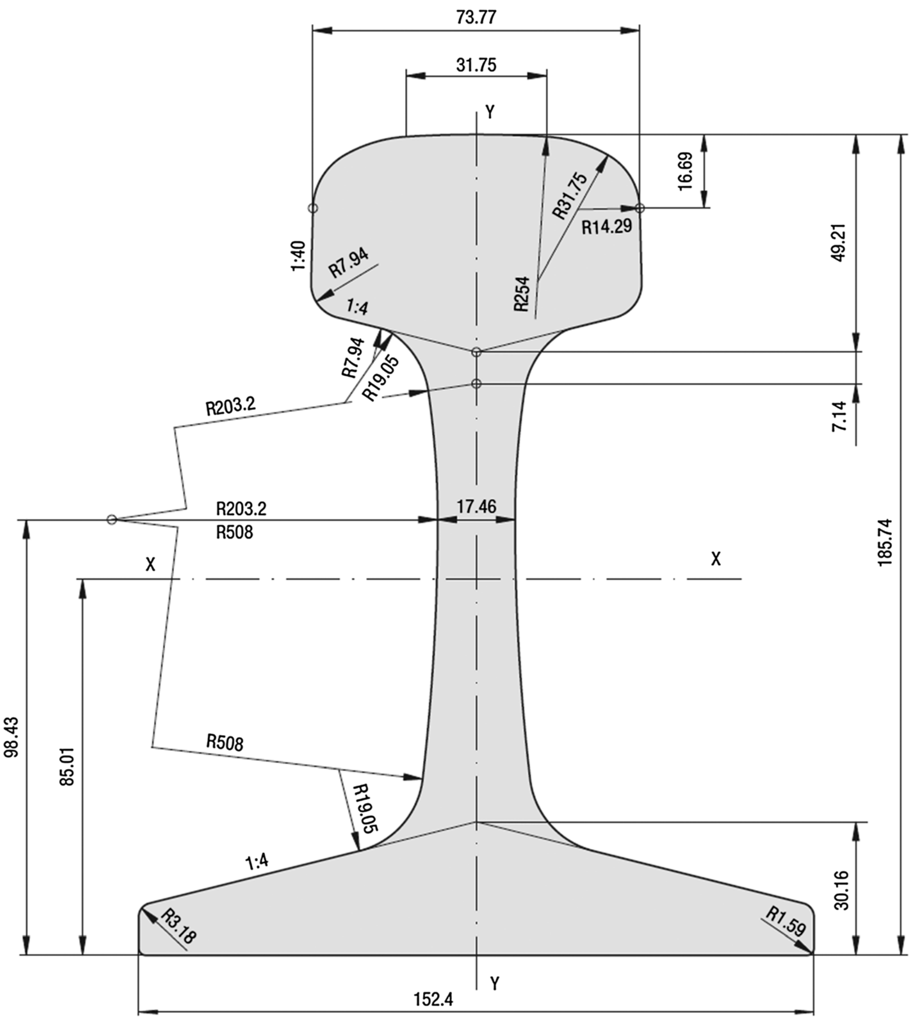

Fig. 6 Cross-section of the rail profile.

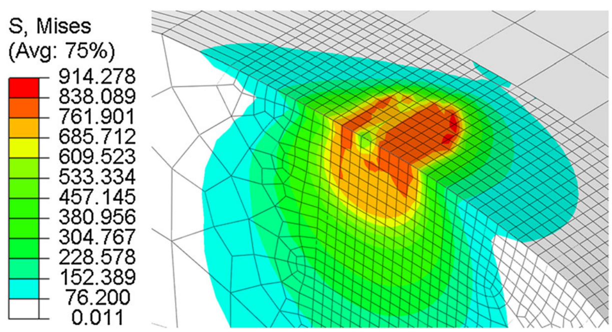

Fig. 7 von Mises stress field in the rail head of the case study.

the elements within the critical zone are considered in finding the highest $S_{\max}^{WT}$. The results of stress and strain components of each integration points at each increment within the loading cycle are then collected. With the use of MATLAB, $S_{\max}^{WT}$ is determined by following Eqs. (6–11).

Figure 10 shows the surface contour plot of $S_{\max}^{WT}$ on the x-y plane at different locations along the depth of the rail head, h. For all calculations, the initial contact position between the wheel and the rail is chosen to be the reference point (0,0,0). Figures 10(a) and 10(b) show that the distributions of the $S_{\max}^{WT}$ on the top surface and 0.5 mm below the top surface of the rail head are not as smooth as those shown in Figs. 10(c) to 10(f). This fact is due to the influence of the friction coefficient on both stress and the strain fields at the contact between the wheel and the rail. Additionally, the transverse location of the highest $S_{\max}^{WT}$ on each surface varies along the depth of the rail head. Comparing $S_{\max}^{WT}$ distribution in Fig. 10(a) to 10(f), the highest $S_{\max}^{WT}$ of the model is 11.589 MPa and it is located at 1.5 mm below the top surface of the rail head; see Fig. 10d.

Figure 11 shows $S_{\max}^{WT}$ versus the depth of the rail head, h on the plane with the highest $S_{\max}^{WT}$. It can be seen that

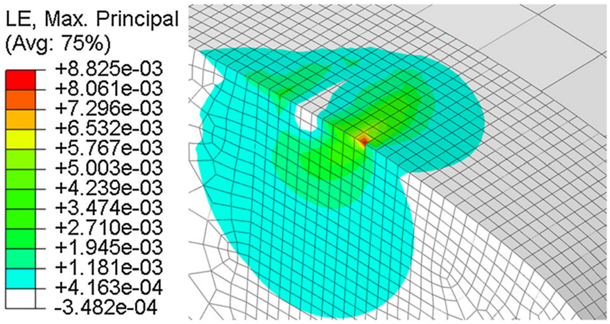

Fig. 8 Maximum principal strain field in the rail head of the case study.

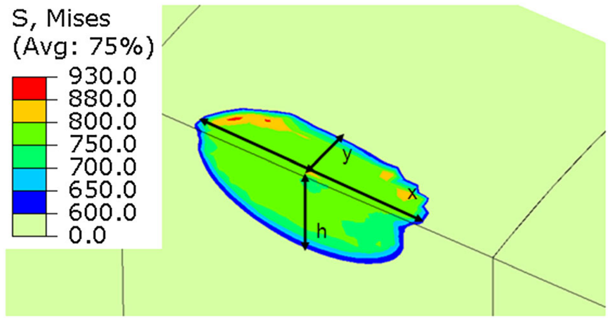

Fig. 9 Critical zone in the rail head of the case study.

$S_{\max}^{WT}$ increases with h until the highest $S_{\max}^{WT}$ is reached. After that, it decreases with h and approaches to zero. Figure 12 shows the distribution of $S_{\max}^{WT}$ on the plane of the highest $S_{\max}^{WT}$ along the transverse direction, y. The results indicate that the transverse location of the highest $S_{\max}^{WT}$ is 1.5 mm from the initial contact position towards the gauge corner. Figure 13 demonstrates the variation of $S_{\max}^{WT}$ along the running direction x on the plane with the highest $S_{\max}^{WT}$. The results clearly demonstrate that the highest $S_{\max}^{WT}$ is around the initial contact position between the wheel and the rail. Combining the results in Figs. 11, 12 and 13, the exact location of the highest $S_{\max}^{WT}$ of the specimen is at (−0.2, 1.5, −1.5) with respect to the reference point. It is worth nothing that the orientation of the candidate critical plane is defined by the two angles θ_v and θ_h, which define the direction cosines of a normal to the candidature plane; see Eqs. (7–9). As mentioned earlier, angles of candidate critical planes from 0° to 360° with the increment of 5° are considered in the calculation for each single integration point. According to Eqs. (7–9), four sets of angles θ_v and θ_h give the same $S_{\max}^{WT}$ value at each single integration point. In another word, two crack surfaces give the same $S_{\max}^{WT}$ value for each single integration point. In current case study, the calculated angles θ_v and θ_h for the orientations of the normal to the crack plane with the highest $S_{\max}^{WT}$ are summarised in Table 1. Additionally, the predicted directions of two crack surfaces, C1 and C2, at the location of the highest $S_{\max}^{WT}$ are illustrated in Fig. 14.

Typically, a rolling contact fatigue crack can be originated from either a small surface crack or sub-surface crack.[36] In the current case study, the results indicate that the crack initiates in the sub-surface of the rail head and propagates on two possible crack surfaces. Both crack surfaces are inclined with a very acute angle of 15° to the running surface of the rail head. The predicted rolling contact fatigue cracks with such orientations have been commonly observed in practice, for example, Fig. 1.[1]

Applying a single parameter to evaluate the stress state in the rail head, the result of the critical position for crack initiation from the von Mises stress method, is different from the SWT method. This is because the SWT method includes the elastic and plastic deformation of the material for fatigue analysis while the von Mises stress does not. It is worth nothing that a reasonable critical zone, which can cover both large von Mises stress and large maximum principal strain values, should be identified for determining the highest maximum SWT parameter and, therefore, for locating the position of crack initiation and crack direction(s). The value of the highest maximum SWT parameter, combined with experimental data via Eq. (5),

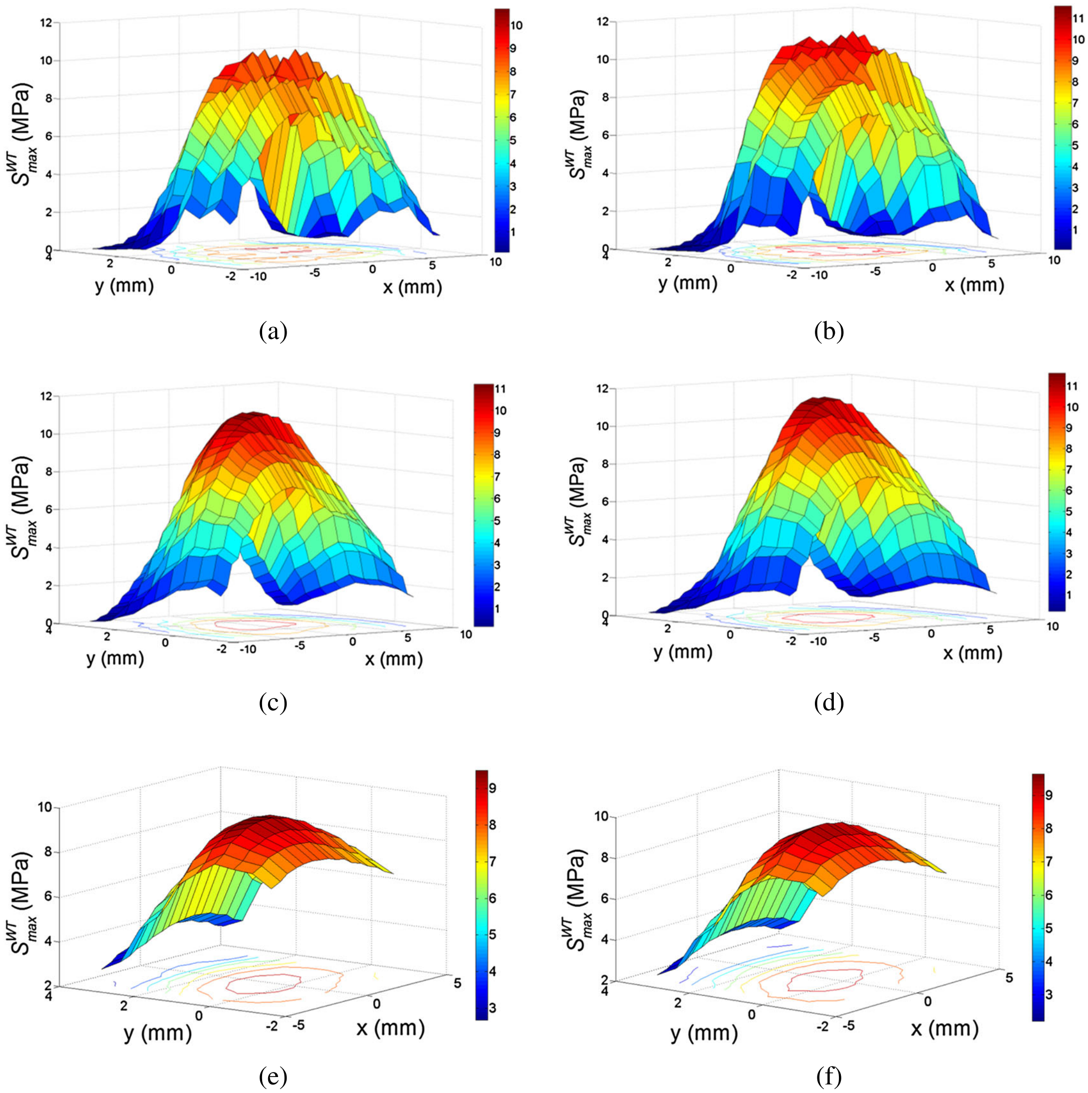

Fig. 10 Surface contour plot of the maximum Smith-Watson-Topper parameter, $S_{\max}^{WT}$, on the *x-y* plane at (a) $h = 0$ mm; (b) $h = 0.5$ mm; (c) $h = 1$ mm; (d) $h = 1.5$ mm; (e) $h = 2$ mm; (f) $h = 2.5$ mm.

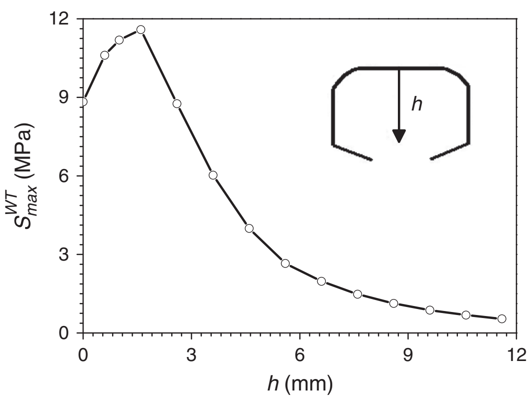

Fig. 11 Distribution of the maximum Smith-Watson-Topper, $S_{\max}^{WT}$, along the depth of the rail head, h, on the plane of the highest $S_{\max}^{WT}$.

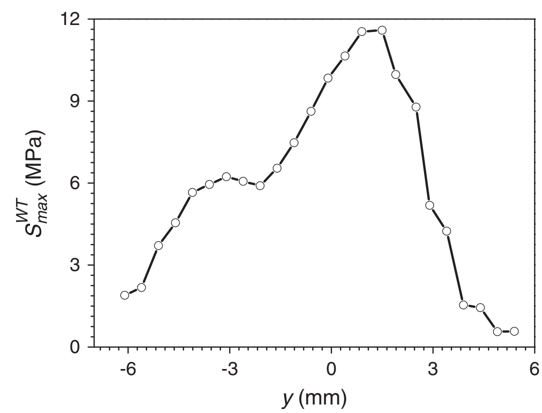

Fig. 12 Distribution of the maximum Smith-Watson-Topper, $S_{\max}^{WT}$, on the plane of the highest $S_{\max}^{WT}$ along the transverse direction, y.

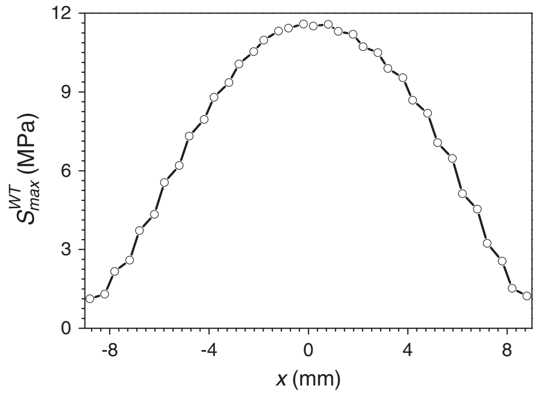

Fig. 13 Distribution of the maximum Smith-Watson-Topper, $S^{WT}_{\max}$, on the plane of the highest $S^{WT}_{\max}$ along the running direction, x.

Table 1 Angles, θ_v and θ_b, of the crack plane at the highest $S^{WT}_{\max}$ of the model.

θ_v	θ_b
15°	85°
15°	265°
195°	95°
195°	275°

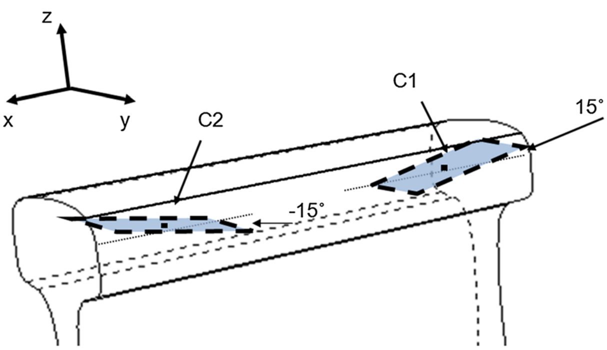

Fig. 14 Illustration of the predicted directions of the crack surfaces, C1 and C2, at the location of the highest $S^{WT}_{\max}$.

can be used to predict the fatigue life. Additionally, the case study demonstrates that to find the highest maximum SWT parameter, the location of fatigue crack initiation and the crack surfaces for crack propagation can also be predicted. Therefore, the maximum SWT parameter is proposed as a single parameter to evaluate the stress state in the rail head for rolling contact fatigue, which is analogous to use of von Mises stress as a single parameter to evaluate the strength of a structure. Practically, knowing the value of the highest maximum SWT parameter in a rail head of a specified railway can provide a quantitative measure about the structural integrity of the rail head without carrying a complicated failure analysis. For example, if the value of the highest maximum SWT parameter in Case A is higher than that in Case B for the same rail, then Case A is more vulnerable to fatigue failure. Actively monitoring the highest maximum SWT parameter in a rail head can provide the information for rail maintenance. This single parameter can also be applied at the design stage of a railway rail. Furthermore, analogous to von Mises stress for strength analysis under static loading, the maximum SWT parameter can be applied to evaluate the fatigue loading state in a generic structure subjected to a cyclic loading.

CONCLUSIONS

To search for a single parameter to evaluate the stress state in the rail head for rolling contact fatigue analysis, the maximum SWT parameter, which is originated from the SWT method for multiaxial fatigue analysis, was analysed in current study. The SWT method includes the contribution of stress, elastic strain and plastic strain components in a multiaxial fatigue analysis. It can predict not only the fatigue life but also the location of the possible rolling contact fatigue and the direction of the initiated fatigue crack, which has been demonstrated successfully in a case study. Consequently, the maximum SWT parameter is proposed as a single parameter to evaluate the stress state in the rail head for rolling contact fatigue analysis. Practically, the value of this single parameter can be applied as an indicator to control the stress state and to maintain the rail in a railway system.

Acknowledgements

The present work has been partly funded by an Australian Research Council Linkage Project (LP110100655) with support from Rio Tinto Iron Ore. The computational simulations were carried out at the NCI National Facility in Canberra, Australia, which is supported by the Australian Commonwealth Government.

REFERENCES

1 Mutton, P. J., Tan, M. and Kapoor, A. (2009) The effect of severe head wear on rolling contact fatigue in heavy haul operations. In: *8th International Conference on Contact Mechanics and Wear of Rail/Wheel Systems*, Firenze, Italy, 15-18 September.

2 Beynon, J. H., Garnham, J. E. and Sawley, K. J. (1996) Rolling contact fatigue of three pearlitic rail steels. *Wear*, **192**, 94–111.

3 Shur, E. A., Bychkova, N. Y. and Trushevsky, S. M. (2005) Physically metallurgy aspects of rolling contact fatigue of rail steels. *Wear*, **258**, 1165–1171.

4 Green, M. R., Rainforth, W. M., Frolish, M. F. and Beynon, J. H. (2007) The effect of microstructure and composition on the

rolling contact fatigue behaviour of cast bainitic steels. *Wear*, **263**, 756–765.
5 Mutton, P. J., Welsby, D. and Alvarez, E. (2009) Wear and rolling contact fatigue behaviour of heat-treated eutectoid and hypereutectoid rail steels under high axle load conditions. In: *8th International Conference on Contact Mechanics and Wear of Rail/Wheel Systems*, Firenze, Italy, 15-18 September.
6 Stock, R. and Pippan, R. (2011) RCF and wear in theory and practice – The influence of rail grade on wear and RCF. *Wear*, **271**, 125–133.
7 Cookson, J. M. and Mutton, P. J. (2011) The role of the environment in the rolling contact fatigue cracking of rails. *Wear*, **271**, 113–119.
8 Tournay H. M. and Mulder J. M. (1996) The transition from the wear to the stress regime. *Wear*, **191**, 107–112.
9 Roney, M. (2005) Common elements of successful heavy haul railways: a worldwide perspective. In: *8th International Heavy Haul Conference*, *Rio de Janeiro*, Brazil, 14-16 June, 221–225.
10 Fröhling, R. D. (2007) Wheel/rail interface management in heavy haul railway operations – applying science and technology. *Veh. Syst. Dyn.*, **45**(7-8), 649–677.
11 Jiang, Y., Xu, B. and Sehitoglu H. (2002) Three-dimensional elastic-plastic stress analysis of rolling contact. *J. Tribol.*, **124**, 699–708.
12 Xu, B. and Jiang, Y. (2002) Elastic-plastic finite element analysis of partial slip rolling contact. *J Tribol.*, **124**, 20–26.
13 Wen, Z., Wu, L., Li, W., Jin, X. and Zhu, M. (2011) Three-dimensional elastic-plastic stress analysis of wheel-rail rolling contact. *Wear*, **271**, 426–436.
14 Seo, J. W., Kwon, S. J., Jun, H. K. and Lee D. H. (2011) Numerical stress analysis and rolling contact fatigue of White Etching Layer on rail steel. *Int. J. Fatigue*, **33**, 203–211.
15 Wen, Z. F., Jin, X. S. and Jiang Y. Y. (2005) Elastic-plastic finite element analysis of non-steady state partial slip wheel-rail rolling contact. *J. Tribol.*, **127**, 713–721.
16 Smith, K. N., Watson, P., Topper, T. H. (1970) A stress-strain function for the fatigue of metals. *J. Mater.*, **5**(4), 767–778.
17 Sum, W. S., Williams, E. J. and Leen S. B. (2005) Finite element critical plane, fatigue life prediction of simple and complex contact configurations. *Int. J. Fatigue*, **27**, 403–416.
18 Zhu, Y., Kang, G., Ding, J. and Zhu, M. (2013) Study on bending fretting fatigue of LZ50 axle steel considering ratchetting by finite element method. *Fatigue Fract. Eng. Mater. Struct.*, **36**, 127–138.
19 Klemenc, J., Janezic, M. and Fajdiga, M. (2012) Modelling the dependency of the Smith-Watson-Topper parameter on the cycles-to-failure using serial hybrid neural networks. *Fatigue Fract. Eng. Mater. Struct.*, **35**, 809–825.
20 Chen, X., Xu, S. and Huang, D. (1999) A critical plane-strain energy density criterion for multiaxial low cycle fatigue life under non-proportional loading. *Fatigue Fract. Eng. Mater. Struct.*, **22**, 679–686.
21 Li, J., Liu, J., Sun, Q., Zhang, Z.-P. and Qiao Y.-J. (2012) A modification of Smith-Watson-Topper damage parameter for fatigue life prediction under non-proportional loading. *Fatigue Fract. Eng. Mater. Struct.*, **35**, 301–316.
22 Kapoor, A. (1997) Wear by plastic ratchetting. *Wear*, **212**, 119–130.
23 Suresh, S. (2002) Fatigue of Materials, 2nd edn. Cambridge University Press, Cambridge, UK.
24 Socie, D. (1987) Multiaxial fatigue damage models. *J. Eng. Mater. Technol.*, **109**(4), 293–298.
25 You, B. R. and Lee, S. B. (1996) A critical review on multiaxial fatigue assessments of metals. *Int. J. Fatigue*, **18**, 235–244.
26 Das, J. and Sivakumar, S. M. (1999) An evaluation of multiaxial fatigue life assessment method for engineering components. *Int. J. Press. Vessels Pip.*, **76**, 741–746.
27 Ringsberg, J. W. (2001) Life prediction of rolling contact fatigue crack initiation. *Int. J. Fatigue*, **23**, 575–586.
28 Szolwinski, M. P. and Farris T. N. (1996) Mechanics of fretting fatigue crack formation. *Wear*, **198**, 93–107.
29 Araujo, J. A. and Nowell, D. (2002) The effect of rapidly varying contact stress fields on fretting fatigue. *Int. J. Fatigue*, **24**, 763–775.
30 Fridrici, V., Fouvry, S., Kapsa, P. and Perruchaut, P. (2005) Prediction of cracking in Ti-6Al-4 V alloy under fretting-wear: use of the SWT criterion. *Wear*, **259**, 300–308.
31 Lykins, C. D., Mall, S. and Jain, V. K. (2001) Combined experimental-numerical investigation of fretting fatigue crack initiation. *Int. J. Fatigue*, **23**, 703–711.
32 Nackenhorst, U. (2004) The ALE-formulation of bodies in rolling contact theoretical foundations and finite element approach. *Comput. Meth. Appl. Mech. Eng.*, **193**, 4299–4322.
33 Chang, C., Wang, C., Chen, B. and Li, L. (2010) A study of a numerical analysis method for the wheel-rail wear of a heavy-haul train. *Proc. Inst. Mech. Eng. Part F J. Rail Rapid Transit*, **224**, 473–482.
34 Abaqus Analysis User's Manual (2010) Version 6.10, Dasssault Systemes Simulia Corp, Providence, RI, USA.
35 Brunel, J. F., Charkaluk, E., Dufrenoy, P. and Demilly, F. (2010) Rolling contact fatigue of railways wheels: influence of steel grade and sliding conditions. *Procedia Eng.*, **2**, 2161–2169.
36 Zerbst, U., Mädler, K. and Hintze, H. (2005) Fracture mechanics in railway applications – an overview. *Eng. Fract. Mech.*, **72**, 163–194.